





Cite this: DOI: 10.1039/d3ta01763j

A strong, biodegradable, and recyclable all-lignocellulose fabricated triboelectric nanogenerator for self-powered disposable medical monitoring†

Xue Shi,^{‡ab} Pengfei Chen,^{‡ab} Kai Han,^a Chengyu Li,^{ab} Renyun Zhang,^{*d}
Jianjun Luo ^{*ab} and Zhong Lin Wang ^{*ac}

The growing demand for fast, reliable, and accessible information in the vastly connected world makes disposable sensors increasingly important. However, reducing their costs, environmental impact, and usability remains challenging. Here, we report a low-cost, biodegradable, and recyclable all-lignocellulosic triboelectric nanogenerator (AL-TENG) for self-powered disposable medical monitoring. Based on a facile *in situ* lignin regeneration & chemical crosslinking modification strategy, a high-performance lignocellulosic bioplastic is synthesized from resource-abundant and renewable biomass for fabricating the AL-TENG. The whole device has a low environmental impact as it can be easily recycled and biodegraded at its end-of-life. Furthermore, a self-powered smart ward system and a self-powered contactless medical monitoring system are developed to improve the convenience for patients and reduce the risk of mutual infection. This work can expand the application of self-powered systems to disposable medical sensing, which may greatly promote the development of intelligent wards and disposable electronics.

Received 24th March 2023

Accepted 11th May 2023

DOI: 10.1039/d3ta01763j

rsc.li/materials-a

1. Introduction

Disposable sensors are easy-to-use, low-cost sensing devices intended for single-shot or short-term measurements. The application areas of such devices are numerous, ranging from agricultural, pharmaceutical, environmental, and food sciences to clinical diagnostics.^{1,2} There is tremendous demand for disposable sensors in the modern medical industry, especially for infectious diseases, since their use can effectively monitor the health state of patients and control the disease within cross-infection.³⁻⁷ However, traditional disposable sensors are usually fabricated from non-degradable plastic, rubber, and metal, and are generally powered by batteries, which is easy to result in high production costs and environmental pollution.⁸⁻¹⁰ To

reduce/eliminate the environmental impact and be commercially viable, it is highly desirable to develop sustainable, degradable, and inexpensive disposable medical sensors for the health monitoring of infectious diseases.

Based on the coupling effect of contact electrification and electrostatic induction, triboelectric nanogenerators (TENGs) have been recently developed as a powerful technology for energy harvesting and self-powered sensing.¹¹⁻¹³ With lots of unique merits such as low-cost, high efficiency, simple structures, and versatile choices of materials,¹⁴⁻¹⁶ TENGs are able to harvest different kinds of mechanical energy in the external environment for realizing large-scale self-powered electronics networks.¹⁷⁻²¹ Moreover, TENGs can also be used as self-powered sensors for tactile, pressure, acceleration, and motion sensing without an additional power supply, which is critical for the development of sustainable sensing systems.²²⁻²⁶ Therefore, the TENG technology will open up broad application prospects in the field of health monitoring, where large amounts of sensing devices should be applied.

Most of the raw materials currently used for fabricating TENGs are non-degradable synthetic plastics, which may cause serious environmental pollution. Lignocellulose is the most abundant natural polymer on earth with an annual production of 170 billion tons.^{27,28} As a sustainable, recyclable, biodegradable, and processable material, it has been widely used in building materials, clothing, functional materials, and smart

^aCAS Center for Excellence in Nanoscience, Beijing Key Laboratory of Micro-Nano Energy and Sensor, Beijing Institute of Nanoenergy and Nanosystems, Chinese Academy of Sciences, Beijing 101400, P. R. China. E-mail: luojianjun@binn.cas.cn

^bSchool of Nanoscience and Technology, University of Chinese Academy of Sciences, Beijing 100049, P. R. China

^cGeorgia Institute of Technology, Atlanta, Georgia 30332-0245, USA. E-mail: zhwang@gatech.edu

^dDepartment of Engineering, Mathematics, and Science Education, Mid Sweden University, Holmgatan 10, SE 85170 Sundsvall, Sweden. E-mail: renyun.zhang@mium.se

† Electronic supplementary information (ESI) available. See DOI: <https://doi.org/10.1039/d3ta01763j>

‡ These authors contributed equally to this work.

materials in electronics.^{29–33} Producing lignocellulose bioplastic (LB) to replace petrochemical-based plastics can effectively reduce greenhouse gas emissions.³⁴ However, traditional approaches for fabricating LB usually require complex processing steps and use toxic chemicals.^{35,36} Additionally, it remains challenging to achieve a good balance between mechanical properties and biodegradability. Therefore, developing a sustainable and simple method to mass-produce lignocellulosic bioplastic for fabricating TENGs will provide a great opportunity for the eco-friendly self-powered system.

Here, we report an effective *in situ* lignin regeneration & crosslinking modification approach to manufacture LB with good biodegradability, flexibility, processability, and mechanical strength. The obtained LB can be completely degraded on the soil surface for 12 days, demonstrating its low environmental impact. Furthermore, a biodegradable all-lignocellulosic triboelectric nanogenerator (AL-TENG) is fabricated, which can be recycled and reduce the waste of resources. Owing to its excellent performance, the AL-TENG is utilized to construct a self-powered smart ward system. By triggering the triboelectric sensing pad, patients can remotely control the equipment in the ward. In addition, a self-powered contactless medical monitoring system that can realize health monitoring and emergency rescue is also demonstrated. This work may provide a promising way for self-powered disposable medical monitoring and the construction of smart wards.

2. Experimental

2.1 Materials and chemicals

Poplar wood powder sieved with 60-mesh was selected as a starting material. Choline chloride ($C_5H_{14}ClNO$, >98%, Sigma-Aldrich), oxalic acid dihydrate ($C_2H_2O_4 \cdot 2H_2O$, >99.5%, Sigma-Aldrich), citric acid (CA) ($C_6H_8O_7$, Sigma-Aldrich), sodium hypophosphite (NaH_2PO_2 , Sigma-Aldrich), carbon powder (C, 99.9%, Sigma-Aldrich) with particle size 30–45 nm, and deionized (DI) water were used for processing the wood powder. The cellulose film was purchased from Weifang Aikang Biotechnology Limited Company and used as a control to measure the mechanical strength.

2.2 Fabrication of the LB

Choline chloride and oxalic acid at a molar ratio of 1 : 1 were mixed and stirred at 80 °C until a transparent liquid was obtained. Poplar wood powder and DES at a 1 : 15 mass ratio were mixed and stirred at 110 °C. The resultant dark brown liquid was stirred at 600 rpm for 2 h by adding DI water (1 : 10 v/v). The cellulose–lignin mixture was vacuum-filtered and washed using DI water to remove residual DES. The DES was recycled by heating the filtered liquid to remove water. Then, CA and sodium hypophosphite were added to the cellulose–lignin mixture, where the mass ratio of poplar powder, CA, and sodium hypophosphite was 10 : 2 : 1. The LB film can be obtained from the cellulose–lignin mixture by a roll-to-roll process after evaporation of water at room temperature (~10 wt% water content). Furthermore, for the preparation of the conductive LB

film, the only difference was the addition of carbon powder to the CA crosslinked cellulose–lignin mixture. The mass ratio of poplar wood and carbon powder was 20 : 1. In the roll-to-roll process, the gap between the two rollers was set at 1.5 mm for the preparation of large-scale LB and 0.5 mm for the preparation of AL-TENG devices.

2.3 Fabrication of the AL-TENG

The obtained LB was used as the dielectric electrification layer. Then, a layer of the conductive LB film with the same size was pasted on the LB as the electrode to fabricate the single-electrode mode TENG. Finally, a Cu wire was attached to the conductive LB for an electric connection.

2.4 Characterization and measurements

Unless otherwise specified, the frequency and pressure were respectively constrained at 1 Hz and 3.5 kPa, and the size of the TENG device was set to $2 \times 2 \times 0.05 \text{ cm}^3$. For electrical measurements, the TENG device was driven using a linear motor (Linmot E1100). A programmable electrometer (Keithley 6514) was used to measure the open-circuit voltage and short-circuit current. The morphology of the LB and UC-LB was observed with a scanning electron microscope (SEM, SU8020, Hitachi). The FTIR spectrum was measured by using a Fourier transform infrared spectrometer (FTIR, VERTEX80v, Bruker). XRD patterns were collected using an Xpert3 Powder diffractometer (operating tube voltage of 40 kV and tube current at 40 mA). The tensile properties of the LB, UC-LB, and cellulose film were measured using an E3000 tester. The dimensions of the samples were $\sim 5 \times 1 \text{ cm}^2$. The surface potential maps and electrostatic forces strength of LB was obtained by Kelvin probe force microscopy (KPFM, Multimode 8, Bruker). The square resistance was measured by using a 4-point probe resistivity measurement system (RTS-9). Thermogravimetric analysis of the LB under air was carried out in the range of 30–800 °C and a ramping rate of 10 °C min^{-1} (TGA, 4000, PerkinElmer). Note that the LB samples were pressed (130 °C, 5 h) for the SEM analysis, FTIR spectra, XRD patterns, mechanical tensile test, and electrical properties.

2.5 Biodegradability test

For the soil biodegradability test, the LB, UC-LB, and PTFE were cut into $20 \times 20 \times 0.05 \text{ mm}^3$ pieces and then buried in the soil at a depth of 5 cm to test the biodegradability. To simulate outdoor testing, the LB, UC-LB, and PTFE were cut into $20 \times 20 \times 0.05 \text{ mm}^3$ pieces and then placed on the soil surface in a thermostatic incubator. The ambient temperature and relative humidity of the degradation experiment were maintained at 30 °C and 60%. Samples were monitored regularly to test their biodegradability.

3. Results and discussion

3.1 Preparation of biodegradable and recyclable LBs

As shown in Fig. 1a, we select green plants that are abundant in nature as raw materials, using an efficient *in situ* lignin

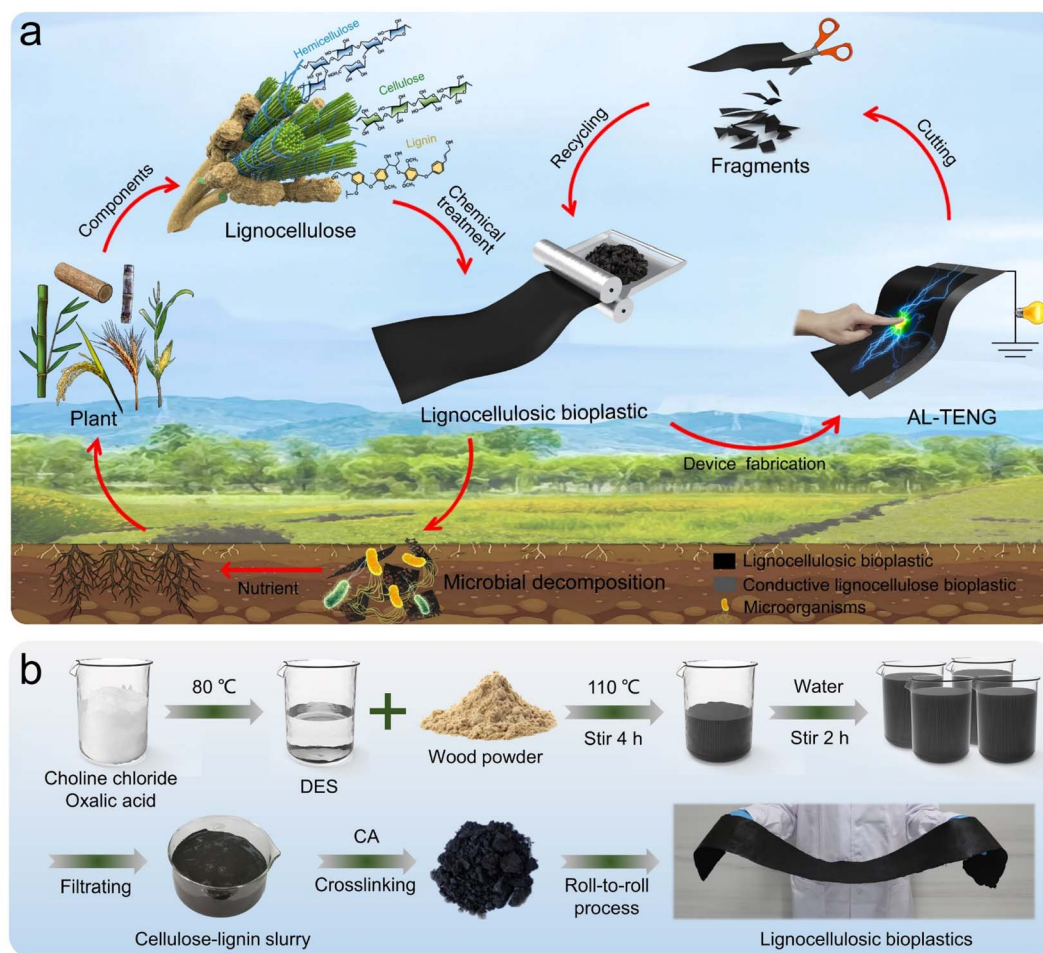


Fig. 1 The preparation of the high-performance LB and AL-TENG. (a) Schematic diagram of biodegradability and recyclability of the LB and AL-TENG. (b) The fabrication process of the LB by the *in situ* lignin regeneration, crosslinking modification, and roll-to-roll process ($115 \times 15 \times 0.15 \text{ cm}^3$).

regeneration & crosslinking modification strategy to fabricate the LB with low-cost, high strength, superior processability, recyclability, and biodegradability. By utilizing the roll-to-roll manufacturing technology, the LB is also easy for large-scale production. The end-of-life LB can be broken back down into the uniform cellulose–lignin slurry by mechanical stirring, allowing it to be reapplied as a recycled material. Unlike most petrochemical plastics, this LB can be biodegraded by microorganisms in the soil, demonstrating a fascinating close-loop cycle feature. By adding low-cost carbon powder in the preparation process, the conductive LB film can also be produced as the electrode material of the TENG. Based on the excellent characteristics of LBs, we have realized a biodegradable and recyclable all-lignocellulosic TENG (AL-TENG), which can be recycled by mechanical disintegration, allowing the material to be reclaimed and used again in the production of AL-TENGs. The biodegradable and recyclable AL-TENG demonstrated here is a strong candidate for replacing the petrochemical plastic-based TENG toward sustainable applications. Meanwhile, the design of AL-TENGs provides a new perspective for intelligent medical active sensing systems. Considering its energy

harvesting and self-powered sensing ability, the AL-TENG may greatly promote the development of the intelligent disposable medical monitoring field.

Fig. 1b shows the schematic of the fabrication process of the LB using an *in situ* lignin regeneration & crosslinking modification method directly from inexpensive and abundant poplar powder. The starting wood material has a mesoporous structure and is mainly made up of cellulose, hemicellulose, and lignin.^{37,38} Among them, lignin serves as a binder that helps to adhere to the cellulose fibers. To deconstruct the loose and porous structure of the poplar wood powder, we used a deep eutectic solvent (DES) consisting of choline chloride (ChCl) and oxalic acid, which can efficiently dissolve the lignin and deconstruct the wood by disrupting the hydrogen bonding between cellulose fibers.^{39–42} The hydrogen bonding interactions ($\text{OH} \cdots \text{Cl}$) formed by ChCl and oxalic acid can reduce the crystallization ability of compounds and keep the DES in a stable liquid state (Fig. S1†). Meanwhile, this configuration facilitates the delocalization of the hydrogen protons in oxalic acid, which can increase the acidity of the DES, as well as improve the dissolution of native lignin and the defibrillation of

the wood.^{43,44} Then we *in situ* regenerate the lignin by adding water, which causes it to deposit and bind to the interconnected cellulose micro/nanofibril network through the formation of hydrogen bonding (Fig. S2†). After filtering and washing this mixture using water to remove residual DES, large quantities of the cellulose–lignin slurry can be obtained. To further improve the physical and mechanical properties of cellulose materials, citric acid (CA) is used as a bond promoter, which is widely used as a safe and environmentally friendly natural adhesive. The CA added to the obtained high solid-content slurry can reinforce the cross-linking of lignin and cellulose.^{45–48} Finally, by evaporating most of the water at room temperature, we can fabricate LBs *via* a simple roll-to-roll process at a large-scale. Fig. S3† shows the obtained LB with a size of $115 \times 15 \times 0.15 \text{ cm}^3$. The structural changes of lignin and cellulose during the preparation of LBs are shown in Fig. S4.† In addition, conductive LBs (C-LBs) can also be prepared by adding conductive carbon powder in the fabrication process.

3.2 Structure and composition of the LB

The *in situ* lignin regeneration & CA chemical crosslinking modification method eliminates the need to separate and isolate lignin and cellulose from materials, which is a simple and low-cost process. Compared with the uncross-linked LB (UC-LB), the LB exhibits a dense and homogeneous structure with a relatively

flat surface (Fig. 2a and b). Lignin is a natural and biodegradable binder that tightly holds the micro/nanofibrils together, enhancing the interactions between them (Fig. 2c and S5a†). The crosslinking reaction produced by the addition of CA can further strengthen the connection between lignin and cellulose, and obtain the LB with a more uniform and dense structure (Fig. 2d and S5b†). To clarify the presence of lignin in the LB and the chemical bonds formed between cellulose, lignin, and CA, we conducted Fourier transform infrared (FTIR) spectroscopy of the natural poplar powder, pure cellulose, UC-LB, and the LB. As shown in Fig. 2e, compared with pure cellulose, the wood powder, UC-LB, and the LB have obvious absorption peaks at 1602, 1508, and 1456 cm^{-1} in the FTIR spectrum, which are attributed to the vibrations of the aromatic skeleton of lignin.⁴⁹ A new absorption peak of the UC-LB also appears at 1733 cm^{-1} , which corresponds to the $\text{C}=\text{O}$ stretching of a carbonyl group, indicating the partial esterification of the cellulose hydroxyl groups by oxalic acid during the DES treatment.⁵⁰ In comparison with the UC-LB, the LB shows a higher absorption band at 1733 cm^{-1} , indicating that the carbonyl peak of the esters formed between CA and the hydroxyl groups in lignocellulose or carboxylic acids from CA appears.^{45,51} The intensity change was also found in the peak at 1200 cm^{-1} , which was assigned to the C–O stretch in esters.^{46,52} The methoxylene group band located at 2952 and 2865 cm^{-1} also increased, which is caused by the cross-linking reaction between

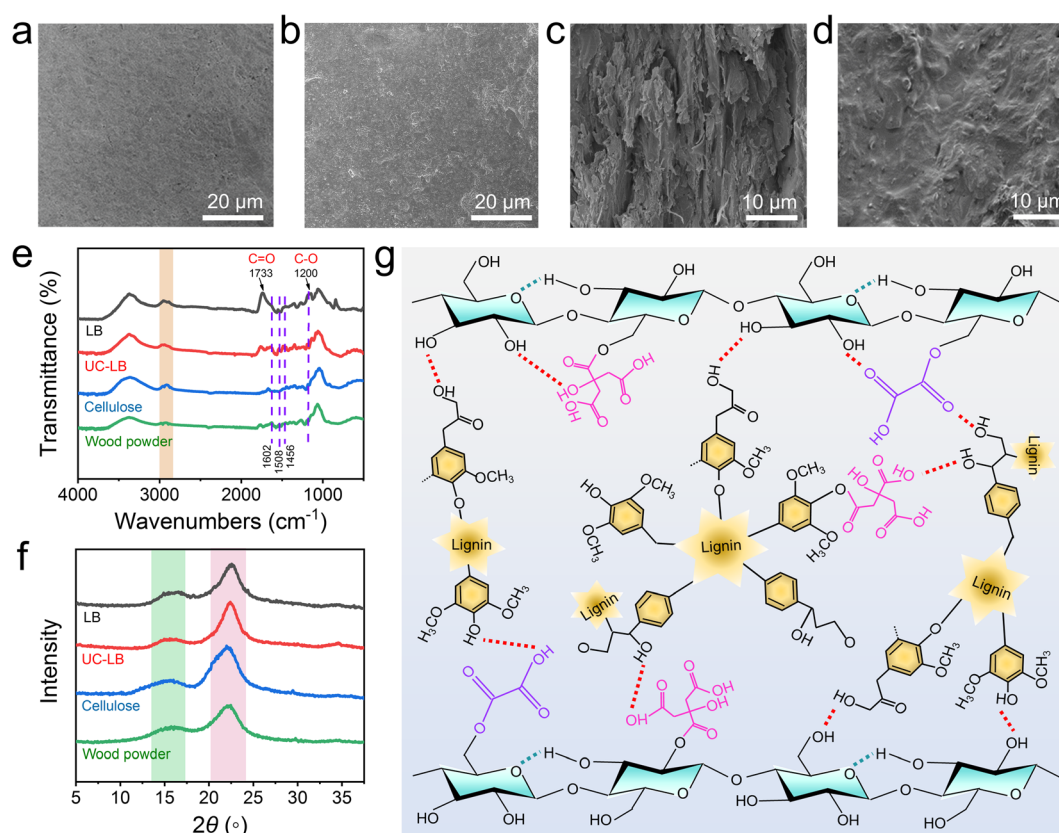


Fig. 2 Structural and compositional characterization of the LB. Top-view SEM images of the (a) UC-LB and (b) LB. Cross-sectional-view magnified SEM images of the (c) UC-LB and (d) LB. (e) FTIR spectra and (f) XRD spectra of the natural wood powder, cellulose, UC-LB, and LB. (g) The interaction between the regenerated lignin, cellulose, and CA.

CA and lignin.⁵³ Meanwhile, X-ray analysis was performed on the LB to evaluate the degree of crystallinity. The X-ray diffraction patterns of wood powder, cellulose, UC-LB, and LB are shown in Fig. 2f. The main diffractive peaks ($2\theta = 15.40^\circ$ and 22.12°) in these samples are practically identical, which are assigned to the 101 and 002 lattice planes of cellulose I.⁵⁴ There is no significant change before and after the *in situ* lignin regeneration & cross-linking modification process, indicating that it has little effect on the crystallinity structure.

The *in situ* lignin regeneration & chemical crosslinking modification method leads to a homogeneous and highly viscous cellulose–lignin slurry, in which lignin and CA fill the spaces within the interconnected cellulose network, resulting in a highly dense structure. Fig. 2g schematically shows the interaction between the regenerated lignin, cellulose, and CA. Besides entanglement among the cellulose micro/nanofibrils *via* hydrogen bonding, the regenerated lignin can also tightly interact with the micro/nanofibrils and oxalic acid by hydrogen bonding ($\text{OH}\cdots\text{HO}$, $\text{COO}\cdots\text{HO}$) and van der Waals forces to form strong cellulose–lignin supramolecular complexes. Meanwhile, the esterification between oxalic acid and cellulose hydroxyl groups can also strengthen the interaction between cellulose and lignin. In addition, CA contains a large number of carboxyl groups and hydroxyl groups, which can not only cause

self-crosslinking of lignin and cellulose by reacting with hydroxyl groups of two macromolecular chains, but also form crosslinking between hydroxyl groups of lignin and cellulose through the formation of ester bonds. It is worth noting that the roll-to-roll process can make the combination of components more fully bonded, endowing the LB with high mechanical strength and excellent multifunctional performance.

3.3 Performance characterization of the LB

The LB exhibits high flexibility and mechanical strength due to the entanglement of the micro/nanofibrils and the adhesion induced by lignin and CA (Fig. 3a). The fabricated LB can be easily rolled, crimped, folded, load-bearing, and retain its morphology without damage. Fig. 3b compares the tensile stress–strain curves of the LB, UC-LB, and cellulose film. All three curves show a linear deformation behavior before tensile failure. Due to the mutual entanglement of the micro/nanofibrils and lignin & CA-induced adhesion, the LB demonstrates an enhanced tensile strength of 99 MPa, which is 2.6 and 8.3 times that of the UC-LB and the cellulose film. As shown in Fig. 3c, complex shapes can be formed *via* compression molding of the cellulose–lignin slurry, including bump shape

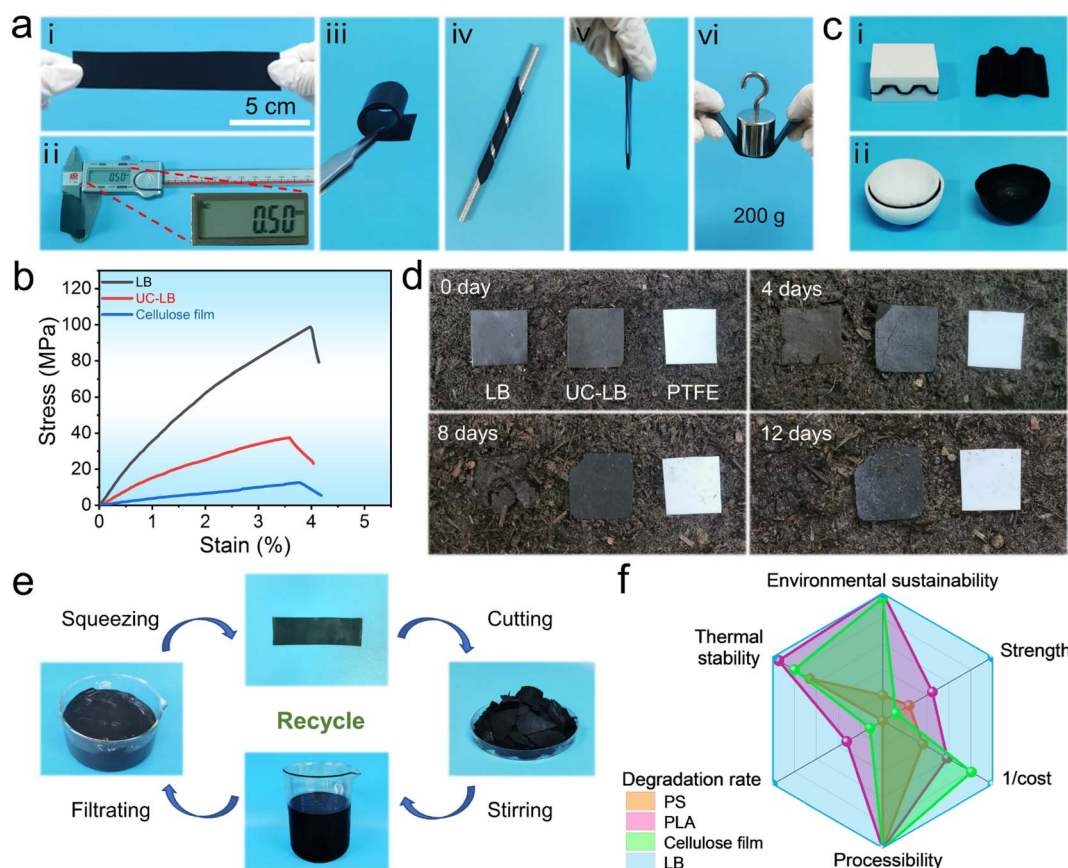


Fig. 3 Performance characterization of the LB. (a) The LB exhibits excellent flexibility and high mechanical strength ($2 \times 12 \times 0.05 \text{ cm}^3$). (b) The tensile stress–strain curves of the cellulose film, UC-LB, and LB. (c) Compression molding of the LB. (d) Biodegradability test of the LB, UC-LB, and PTFE on the soil surface ($2 \times 2 \times 0.05 \text{ cm}^3$). (e) The recyclability of the LB. (f) Radar plots comparing the performance of LB, cellulose film, PLA, and PS, in which the results are normalized by the maximum value of each characteristic.

and hemispherical shell shape structures, demonstrating its excellent processability.

The LB also exhibits excellent biodegradability in the natural environment. For comparison, we placed sheets of the LB, UC-LB, and polytetrafluoroethylene (PTFE) on the soil surface, and monitored their morphology over time to determine their degradability (Fig. 3d). Soil contains a large number of microorganisms (for example, bacteria and fungi), which can directly attack and digest the cellulose and lignin macromolecules of bioplastic.^{55,56} It can be observed that the LB became cracked and fragmented after 4 days, and its original structure completely degraded after 12 days. The UC-LB was near completely biodegraded after 3 months (Fig. S6†). In contrast, the PTFE retained its original shape without any change after a few months, demonstrating that it cannot be degraded in the natural environment. Additionally, when placed in the soil at a depth of 5 cm, the original structure of LB can even undergo complete degradation after 2 days (Fig. S7†). As shown in Fig. S8,† the LB did not show any changes after more than 10 months, indicating its good stability in a real environment. It is worth noting that the LB can be derived from various biomass

feedstocks, such as wheat straw, rice straw, corn straw, bagasse, and bamboo, which have similar FTIR absorption peaks and can be fully biodegraded within 12 days, proving that the LBs prepared from different plants have similar composition (Fig. S9–S11†).

The LB also exhibits good recyclability. At the end of its lifetime, we can break the LB back down into a uniform cellulose–lignin slurry by mechanical cutting and stirring for recycled use (Fig. 3e). Using the same treatment method, the C-LB can also be recycled while maintaining the conductivity (Fig. S12†). In addition, the DES used in the preparation process can also be recovered by simply collecting the filtrate and evaporating the water (Fig. S13†). We took a further step to comprehensively compare the LB, cellulose film, polylactic acid (PLA), and polystyrene (PS) in other parameters, as summarized by the results in Fig. 3f, in which the results are normalized by the maximum value of each characteristic. The LB shows great advantages over the two types of plastic film and cellulose film in all five performance indexes, including environmental sustainability, strength, cost, processability, degradation, and

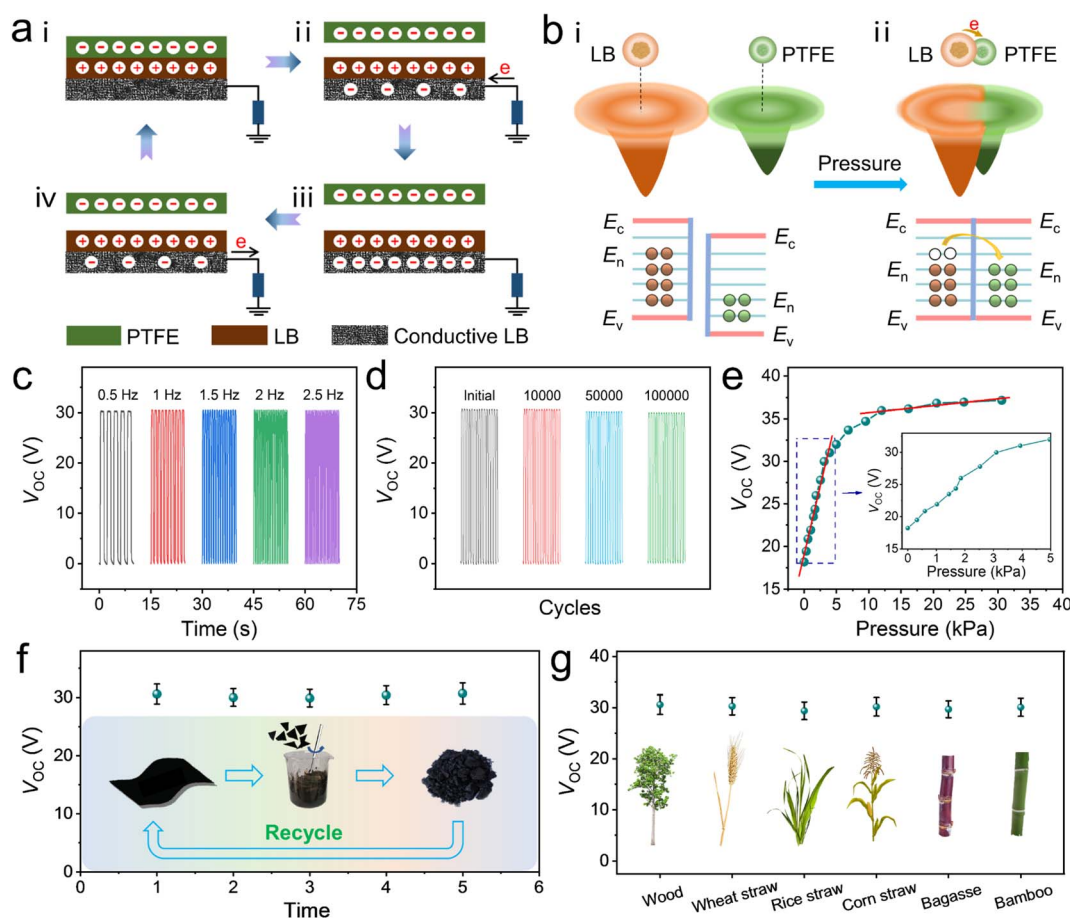


Fig. 4 The working principle and electrical performance of the AL-TENG. (a) Schematic diagram of the working principle of the AL-TENG. (b) Electron cloud model and charge transfer for LB and PTFE: before contact and in contact. (c) V_{OC} of the AL-TENG at frequencies of 0.5, 1, 1.5, 2, and 2.5 Hz. (d) Stability of the AL-TENG at an operating frequency of 1 Hz. (e) V_{OC} of the AL-TENG with increasing pressure. Inset: enlarged view in the low-pressure region. (f) The V_{OC} of the recycled AL-TENG. The inset shows the flow chart of the recycling of the AL-TENG. (g) V_{OC} of the AL-TENG prepared from different kinds of plants.

thermal stability, showing the great potential to replace widely used petrochemical plastics (Fig. S14 and Table S1†).

3.4 The working principles and electrical performance of the AL-TENG

Based on the excellent properties of the LB, high-performance AL-TENGs can be prepared. The cross-sectional-view SEM image of the AL-TENG sensor is shown in Fig. S15,† with LB in the upper layer and C-LB in the lower layer. Fig. 4a shows the working principle of the AL-TENG in single-electrode mode. Taking PTFE as the free-moving object, when the PTFE contact with the LB under an external mechanical force, negative triboelectric charges are generated on the PTFE while positive ones are generated on the LB (i). When the PTFE gradually moves away from the LB, the potential difference between the two surfaces will gradually increase, leading to an electron flow from the ground to the conductive LB through the external circuit (ii). This transient flow of the electrons continues until the PTFE and LB are completely separated (iii). When the PTFE approaches the LB again, the free electrons flow from the electrode to the ground until the PTFE and LB are in contact (iv). When the contact-separation motion between the PTFE and LB is repeated, the alternative current will be formed continuously. The potential distribution of the AL-TENG at different states obtained by COMSOL simulation is shown in Fig. S16.† Fig. 4b illustrates the electron cloud distribution and charge transfer behavior of LB and PTFE at the atomic level, both prior to and during contact. Prior to the atomic contact of the LB and PTFE, their respective electron clouds remain separated without overlap. The potential well binds the electrons and stops them from freely escaping. Owing to the different valence band and conduction band structures of LB and PTFE, the occupied surface states in LB have higher energy than the unoccupied surface states of PTFE (Fig. 4b(i)). Once the LB and PTFE physically contact, the electron clouds overlap between the two atoms to form an ionic or covalent bond. The initial single potential wells become an asymmetric double-well potential, and some of the electrons could transfer from LB's surface to the surface of PTFE, leading to contact electrification (Fig. 4b(ii)). Such electrons will not transfer back to LB even after LB and PTFE are separated, resulting in net positive electrostatic charges on LB and negative electrostatic charges on PTFE. Furthermore, the surface potential of LB before and after contact electrification with PTFE was examined using KPFM (Fig. S17†).

To quantify the electrical output performance of the AL-TENG, a commercial PTFE film was used to produce the relative contact-separation movement with the TENG device (area, $2 \times 2 \text{ cm}^2$). Unless otherwise specified, LB films are made from poplar powder. At a contact pressure of 3.5 kPa, the AL-TENG produced the output performance with an open-circuit voltage (V_{OC}) of 31 V, short-circuit current (I_{SC}) of 0.2 μA , and charge transfer amount (Q_{SC}) of 8 nC (Fig. S18a–c†). Meanwhile, to evaluate the effective output power of the AL-TENG, the output voltage was measured with different resistances applied as the external load. As shown in Fig. S18d† under an external load

resistance of 80 M Ω , the maximum peak output power density of 10 mW m^{-2} can be achieved. To study the delay time of the AL-TENG on external pressure, the V_{OC} of the AL-TENG at various frequencies was measured. An increase in frequency has nearly no effect on the V_{OC} of the AL-TENG (Fig. 4c). As shown in Fig. 4d, the output voltage of the AL-TENG only has a little decay under 100 000 consecutive contact-separation cycles, demonstrating its outstanding stability and durability. Fig. 4e shows the relationship between the V_{OC} and the input pressure from 0 to 30 kPa. As the contact pressure increases, the V_{OC} increases and finally saturates. When the applied pressure is in the low-pressure region (<5 kPa), the AL-TENG exhibits high sensitivity with excellent linearity. Once the pressure exceeds 5 kPa, the pressure sensitivity drops, but still has good linearity. These results reveal that the AL-TENG possesses superior electrical performance and could have great potential in the self-powered sensing field.

Benefiting from the good recyclability of the LB, the fabricated AL-TENG can also be recycled and reprocessed, while maintaining its electrical output performance. As shown in Fig. 4f and S19,† the V_{OC} and the I_{SC} of the AL-TENG only have a negligible change when reusing the LB five times. The AL-TENG can be sheared and mechanically stirred at its end-of-life to obtain the uniform cellulose–lignin slurry for re-application. Moreover, when using other kinds of the plant (including wood, wheat straw, rice straw, corn straw, bagasse, and bamboo) as raw materials, similar electrical output performance could be observed, proving the universality of our method for fabricating AL-TENGs (Fig. 4g and S20†).

3.5 Application of the AL-TENG in smart ward and medical monitoring

Due to its good biodegradability and recyclability, the AL-TENG has great application potential in self-powered disposable medical monitoring. Fig. 5a illustrates the TENG-based self-powered smart ward, which can utilize human motion to control the electrical apparatus in the ward and monitor the patient's status. The working mechanism of the self-powered smart ward system is shown in Fig. 5b. When touching the AL-TENG sensor array with human hands, it can convert the mechanical energy into an electrical signal. Through WIFI transmission and signal control, the facilities in the ward can be remotely controlled by the patient. Fig. 5c–e exhibit the photograph of the remote-control process of the intelligent appliance system. By integrating multiple AL-TENGs in one control pad, different control instructions can be simultaneously realized. As shown in Fig. 5c, multiple AL-TENG sensing units are fixed to the acrylic support plate. The size of each unit is $2 \times 2 \text{ cm}^2$, and the distance between two adjacent units is 0.15 cm. When touching the self-powered control pad with the human finger, an electrical signal is generated. Then, the electrical signal can be wirelessly transmitted through the signal acquisition and process system, which is composed of a circuit controller, a relay, and a wireless transmitter (Fig. 5d). After receiving the wireless signal, corresponding appliances could be accurately controlled through the signal conversion and control system



Fig. 5 Application of the AL-TENG in smart ward and medical monitoring. (a) Schematic diagram of the TENG-based self-powered smart ward. (b) Schematic diagram of the self-powered smart ward system. (c)–(e) Demonstration photographs of the wireless control system based on the AL-TENG: (c) AL-TENG sensor array, (d) signal control circuit, and (e) smart appliances. (f) Demonstration of the self-powered contactless medical monitoring system. (g) and (h) Operating interface of the self-powered contactless medical monitoring system. (i) Screenshot of the mobile phone showing the emergency calls and messages.

(Fig. 5e). Movie S1† shows the operation of the lamp, curtains, and air conditioner, which are remotely controlled by triggering the AL-TENG sensing array with the human finger, demonstrating the effectiveness and simplicity of our system.

Contactless monitoring systems that use disposable sensors to monitor the health of patients with infectious diseases can greatly reduce the risk of infection. The AL-TENG with recyclability and degradability can be utilized as a self-powered disposable tactile sensor, making it a good candidate for realizing contactless medical monitoring. Fig. 5f shows the self-

powered contactless medical monitoring system that can realize health monitoring and emergency rescue, consisting of the AL-TENG sensing module, signal control circuit, and monitoring equipment. To simultaneously monitor and record different symptoms of patients, the AL-TENG sensing array containing 8 AL-TENG units is used (Fig. S21†). Fig. S22† demonstrates the circuit boards of the signal acquisition, processing, relay, and wireless transmission modules. The enlarged view of the system interface is shown in Fig. 5g. When touching the AL-TENGs representing different symptoms,

corresponding output voltage signals will be produced to record the patient's health condition and displayed on the program interface in real-time (Fig. 5h). If the patient needs medical assistance, warning information will also be issued, and emergency calls and messages can be wirelessly sent to specific mobile phones *via* WIFI transmission (Fig. 5i). Movie S2† demonstrates the real-time health condition monitoring process, indicating the accuracy and reliability of our self-powered medical monitoring system. Overall, these results demonstrate the practicability of the AL-TENG in self-powered disposable medical monitoring and reduce the risk of mutual infection between doctors and patients.

4. Conclusions

In summary, we developed a strong, biodegradable, and recyclable all-lignocellulosic triboelectric nanogenerator for self-powered disposable sensing in the medical field. The lignocellulosic bioplastic with excellent mechanical strength, processibility, and biodegradability was prepared using a facile *in situ* lignin regeneration & crosslinking modification method. Combined with the simple roll-to-roll manufacturing process, the LB is also easy for large-scale production. More importantly, the AL-TENG has a low environmental impact since it can be recycled for reuse and biodegraded in the natural environment. As demonstrated, the AL-TENG is adopted to construct a self-powered self-powered smart ward system to improve the convenience for patients. Furthermore, a self-powered contactless medical monitoring system was also realized for remotely monitoring the health condition of patients and reducing the risk of cross-infection between patients and medical staff. This recyclable and green manufacturing approach for fabricating AL-TENGs provides new opportunities for the development of the environmentally-friendly and cost-effective disposable medical sensing industry.

Author contributions

Xue Shi: conceptualization, methodology, data curation, investigation, writing – original draft, writing – review & editing. Pengfei Chen: methodology, data curation, investigation, writing – original draft. Kai Han: visualization, investigation, writing – original draft. Chengyu Li: visualization, investigation. Renyun Zhang: supervision, writing – original draft. Jianjun Luo and Zhong Lin Wang: conceptualization, supervision, writing – original draft, writing – review & editing.

Conflicts of interest

The authors declare no conflict of interest.

Acknowledgements

This research was supported by the National Natural Science Foundation of China (No. 52002028, 52192610, and 22109051), National Key R & D Project from Minister of Science and

Technology (No. 2021YFA0202704), and Beijing Municipal Science & Technology Commission (No. Z171100002017017).

References

- 1 C. Dincer, R. Bruch, E. Costa-Rama, M. T. Fernandez-Abedul, A. Merkoci, A. Manz, G. A. Urban and F. Guder, *Adv. Mater.*, 2019, **31**, 1806739.
- 2 A. J. Killard, *Curr. Opin. Electrochem.*, 2017, **3**, 57.
- 3 P. Mostafalu, A. Tamayol, R. Rahimi, M. Ochoa, A. Khalilpour, G. Kiaee, I. K. Yazdi, S. Bagherifard, M. R. Dokmeci, B. Ziaie, S. R. Sonkusale and A. Khademhosseini, *Small*, 2018, **14**, 1703509.
- 4 J. Kim, M. Kim, M. S. Lee, K. Kim, S. Ji, Y. T. Kim, J. Park, K. Na, K. H. Bae, H. K. Kim, F. Bien, C. Y. Lee and J. U. Park, *Nat. Commun.*, 2017, **8**, 14997.
- 5 Y. H. Chen, S. Y. Lu, S. S. Zhang, Y. Li, Z. Qu, Y. Chen, B. W. Lu, X. Y. Wang and X. Feng, *Sci. Adv.*, 2017, **3**, e1701629.
- 6 J. S. Gootenberg, O. O. Abudayyeh, J. W. Lee, P. Essletzbichler, A. J. Dy, J. Joung, V. Verdine, N. Donghia, N. M. Daringer, C. A. Freije, C. Myhrvold, R. P. Bhattacharyya, J. Livny, A. Regev, E. V. Koonin, D. T. Hung, P. C. Sabeti, J. J. Collins and F. Zhang, *Science*, 2017, **356**, 438.
- 7 F. Guder, A. Ainla, J. Redston, B. Mosadegh, A. Glavan, T. J. Martin and G. M. Whitesides, *Angew. Chem., Int. Ed.*, 2016, **55**, 5727.
- 8 C. M. Rochman, M. A. Browne, B. S. Halpern, B. T. Hentschel, E. Hoh, H. K. Karapanagioti, L. M. Rios-Mendoza, H. Takada, S. Teh and R. C. Thompson, *Nature*, 2013, **494**, 169.
- 9 E. Kim, Y. N. Xia and G. M. Whitesides, *Nature*, 1995, **376**, 581.
- 10 H. L. Shao, J. Chung, K. Lee, L. Balaj, C. Min, B. S. Carter, F. H. Hochberg, X. O. Breakefield, H. Lee and R. Weissleder, *Nat. Commun.*, 2015, **6**, 6999.
- 11 F. R. Fan, Z. Q. Tian and Z. L. Wang, *Nano Energy*, 2012, **1**, 328.
- 12 Z. L. Wang, *Mater. Today*, 2017, **20**, 74.
- 13 Z. L. Wang and A. C. Wang, *Mater. Today*, 2019, **30**, 34.
- 14 R. Hinchet, H. J. Yoon, H. Ryu, M. K. Kim, E. K. Choi, D. S. Kim and S. W. Kim, *Science*, 2019, **365**, 491.
- 15 J. J. Luo and Z. L. Wang, *EcoMat*, 2020, **2**, e12059.
- 16 Z. Wang, W. L. Liu, W. C. He, H. Y. Guo, L. Long, Y. Xi, X. Wang, A. P. Liu and C. G. Hu, *Joule*, 2021, **5**, 441.
- 17 X. J. Li, J. J. Luo, K. Han, X. Shi, Z. W. Ren, Y. Xi, Y. B. Ying, J. F. Ping and Z. L. Wang, *Nat. Food*, 2022, **3**, 133.
- 18 Q. F. Shi, Z. X. Zhang, T. Y. Y. He, Z. D. Sun, B. J. Wang, Y. Q. Feng, X. C. Shan, B. Salam and C. Lee, *Nat. Commun.*, 2020, **11**, 4609.
- 19 H. Yang, Y. K. Pang, T. Z. Bu, W. B. Liu, J. J. Luo, D. D. Jiang, C. Zhang and Z. L. Wang, *Nat. Commun.*, 2019, **10**, 2309.
- 20 X. D. Yang, L. Xu, P. Lin, W. Zhong, Y. Bai, J. J. Luo, J. Chen and Z. L. Wang, *Nano Energy*, 2019, **60**, 404.
- 21 J. H. Zhang, Z. Li, J. Xu, J. Li, K. Yan, W. Cheng, M. Xin, T. Zhu, J. Du, S. Chen, X. An, Z. Zhou, L. Cheng, S. Ying,

- J. Zhang, X. Gao, Q. Zhang, X. Jia, Y. Shi and L. Pan, *Nat. Commun.*, 2022, **13**, 5839.
- 22 K. Dong, X. Peng, J. An, A. C. Wang, J. J. Luo, B. Z. Sun, J. Wang and Z. L. Wang, *Nat. Commun.*, 2020, **11**, 2868.
- 23 J. J. Luo, W. Tang, F. R. Fan, C. F. Liu, Y. K. Pang, G. Z. Cao and Z. L. Wang, *ACS Nano*, 2016, **10**, 8078.
- 24 Z. M. Wang, J. An, J. H. Nie, J. J. Luo, J. J. Shao, T. Jiang, B. D. Chen, W. Tang and Z. L. Wang, *Adv. Mater.*, 2020, **32**, 2001466.
- 25 Y. Lu, H. Tian, J. Cheng, F. Zhu, B. Liu, S. Wei, L. Ji and Z. L. Wang, *Nat. Commun.*, 2022, **13**, 1401.
- 26 J. Luo, Z. Wang, L. Xu, A. C. Wang, K. Han, T. Jiang, Q. Lai, Y. Bai, W. Tang, F. R. Fan and Z. L. Wang, *Nat. Commun.*, 2019, **10**, 5147.
- 27 D. Klemm, B. Heublein, H. P. Fink and A. Bohn, *Angew. Chem., Int. Ed. Engl.*, 2005, **44**, 3358.
- 28 T. E. Amidon and S. Liu, *Biotechnol. Adv.*, 2009, **27**, 542.
- 29 L. A. Berglund and I. Burgert, *Adv. Mater.*, 2018, **30**, 1704285.
- 30 Y. P. Chen, J. Z. Fu, B. K. Dang, Q. F. Sun, H. Q. Li and T. Y. Zhai, *ACS Nano*, 2020, **14**, 2036.
- 31 C. Yan, J. Wang, W. Kang, M. Cui, X. Wang, C. Y. Foo, K. J. Chee and P. S. Lee, *Adv. Mater.*, 2014, **26**, 2022.
- 32 M. T. Chorsi, E. J. Curry, H. T. Chorsi, R. Das, J. Baroody, P. K. Purohit, H. Ilies and T. D. Nguyen, *Adv. Mater.*, 2019, **31**, e1802084.
- 33 L. Wang, K. Wang, Z. Lou, K. Jiang and G. Shen, *Adv. Funct. Mater.*, 2018, **28**, 1804510.
- 34 Q. Q. Xia, C. J. Chen, Y. G. Yao, J. G. Li, S. M. He, Y. B. Zhou, T. Li, X. J. Pan, Y. Yao and L. B. Hu, *Nat. Sustain.*, 2021, **4**, 627.
- 35 H. B. Yue, Y. D. Cui, P. S. Shuttleworth and J. H. Clark, *Green Chem.*, 2012, **14**, 2009.
- 36 D. W. Zhao, Y. Zhu, W. K. Cheng, W. S. Chen, Y. Q. Wu and H. P. Yu, *Adv. Mater.*, 2021, **33**, 2000619.
- 37 Y. Yang, D. Tilman, C. Lehman and J. J. Trost, *Nat. Sustain.*, 2018, **1**, 686.
- 38 A. Venkateshaiah, J. Y. Cheong, S. H. Shin, K. P. Akshaykumar, T. G. Yun, J. Bae, S. Waclawek, M. Cernik, S. Agarwal, A. Greiner, V. V. T. Padil, I. D. Kim and R. S. Varma, *Green Chem.*, 2020, **22**, 1198.
- 39 O. S. Hammond, K. J. Edler, D. T. Bowron and L. Torrente-Murciano, *Nat. Commun.*, 2017, **8**, 14150.
- 40 S. Hong, X. J. Shen, B. Pang, Z. Xue, X. F. Cao, J. L. Wen, Z. H. Sun, S. S. Lam, T. Q. Yuan and R. C. Sun, *Green Chem.*, 2020, **22**, 1851.
- 41 D. Arnodo, S. Ghinato, S. Nejrotti, M. Blangetti and C. Prandi, *Chem. Commun.*, 2020, **56**, 2391.
- 42 J. A. Sirvio, M. Visanko and H. Liimatainen, *Biomacromolecules*, 2016, **17**, 3025.
- 43 X. Z. Qiao, L. Liu, D. K. Yu, H. T. Yu, Y. B. Zhang, Z. M. Xue and T. C. Mub, *Green Chem.*, 2019, **21**, 5291.
- 44 D. Zhao, Y. Zhu, W. Cheng, G. Xu, Q. Wang, S. Liu, J. Li, C. Chen, H. Yu and L. Hu, *Matter*, 2020, **2**, 390.
- 45 D. Ando and K. Umemura, *Polymers*, 2020, **13**, 58.
- 46 H. M. C. Azeredo, C. Kontou-Vrettou, G. K. Moates, N. Wellner, K. Cross, P. H. F. Pereira and K. W. Waldron, *Food Hydrocolloids*, 2015, **50**, 1.
- 47 M. M. Hassan, N. Tucker and M. J. Le Guen, *Carbohydr. Polym.*, 2020, **230**, 115675.
- 48 X. Cui, T. Honda, T. A. Asoh and H. Uyama, *Carbohydr. Polym.*, 2020, **230**, 115662.
- 49 Y. N. Li, Y. Z. Liu, W. S. Chen, Q. W. Wang, Y. X. Liu, J. Li and H. P. Yu, *Green Chem.*, 2016, **18**, 1010.
- 50 H. Q. Wang, J. C. Li, X. H. Zeng, X. Tang, Y. Sun, T. Z. Lei and L. Lin, *Cellulose*, 2020, **27**, 1301.
- 51 K. Umemura, T. Ueda, S. S. Munawar and S. Kawai, *J. Appl. Polym. Sci.*, 2012, **123**, 1991.
- 52 S. S. Kusumah, K. Umemura, K. Yoshioka, H. Miyafuji and K. Kanayama, *Ind. Crop. Prod.*, 2016, **84**, 34.
- 53 X. He, F. Luzi, W. Yang, Z. Xiao, L. Torre, Y. Xie and D. Puglia, *ACS Sustain. Chem. Eng.*, 2018, **6**, 9966.
- 54 M. W. Zhu, J. W. Song, T. Li, A. Gong, Y. B. Wang, J. Q. Dai, Y. G. Yao, W. Luo, D. Henderson and L. B. Hu, *Adv. Mater.*, 2016, **28**, 5181.
- 55 Y. H. Jung, T. H. Chang, H. Zhang, C. Yao, Q. Zheng, V. W. Yang, H. Mi, M. Kim, S. J. Cho, D. W. Park, H. Jiang, J. Lee, Y. Qiu, W. Zhou, Z. Cai, S. Gong and Z. Ma, *Nat. Commun.*, 2015, **6**, 7170.
- 56 K. Sanderson, *Nature*, 2011, **474**, S12.